FI SEVIER

Contents lists available at ScienceDirect

# Powder Technology

journal homepage: www.elsevier.com/locate/powtec



# Removal of emulsified oil from water by inverse fluidization of hydrophobic aerogels

Ding Wang, Trent Silbaugh, Robert Pfeffer\*, Y.S. Lin

School of Mechanical, Aerospace, Chemical and Materials Engineering, Arizona State University, Tempe, AZ, 85287, USA

## ARTICLE INFO

Article history:
Received 29 January 2010
Received in revised form 13 May 2010
Accepted 17 May 2010
Available online 1 July 2010

Keywords: Hydrophobic silica aerogels Inverse fluidization Wastewater Oil-in-water emulsion Tween 80

# ABSTRACT

Different size ranges of surface-treated hydrophobic silica aerogels (Nanogel®) provided by Cabot Corporation are fluidized by a downward flow of an oil-in-water emulsion in an inverse fluidization mode. Surface areas, pore size distributions, and pore diameters are investigated by using BET and contact angle is measured by a goniometer. The hydrodynamics characteristics of the Nanogel granules of different size ranges are studied by measuring the pressure drop and bed expansion as a function of superficial water velocity. The density of the Nanogel granules is calculated from the plateau pressure drop after the bed is fully fluidized. The oil removal efficiency of a dilute (1000 ppm COD or lower), stabilized (using the emulsifier Tween 80) oil-in-water emulsion and the capacity of the Nanogel granules in the inverse fluidized bed are also studied. A model was developed to predict the inverse fluidized bed experimental results based on equilibrium and kinetic batch measurements of the Nanogel granules and the stabilized oil-in-water emulsion. The results show that the major factors which affect the oil removal efficiency and capacity are the size of the nanogel granules, bed height, fluid superficial velocity and the proportion of emulsifier in the oil-in-water emulsion. The Nanogel particles can absorb as much as 2.8 times their weight of oil by the inverse fluidization process.

© 2010 Elsevier B.V. All rights reserved.

# 1. Introduction

One of the most challenging environmental problems today is the removal of oil and other organic contaminants from industrial wastewater and storm water. A large amount of oil discharged into the aquatic ecosystem can cause serious environmental problems, including clogging of sewage treatment plants, adversely affecting the aquatic biota, and increasing biochemical oxygen demand due to the large amount of bacteria necessary to decompose the oil. Oils that exist in contaminated waters can be classified as light hydrocarbons, heavy hydrocarbons, lubricants and cutting fluids, non-emulsified oils such as greases and emulsified oil such as water-soluble oil, and fats found in both plants and animals [1]. Major industrial sources of oily waste include petroleum refining and petrochemical plants [2], steel manufacturing and metal working [3], vehicle repair, and other manufacturing plants. Major municipal sources of oil which contain up to 36% of oily substances are derived from vegetable and animal oils in kitchen and human wastes [4].

Current technologies for oil removal from wastewater include chemical treatment, gravity separators such as the American Petroleum Institute (API) separators [5], gas floatation devices [6], adsorption or absorption by a variety of sorbents such as activated carbon [7], membrane filtration [8,9], and biological treatment [10,11]. Generally, an oil and water mixture can be classified as: free oil, with oil droplets

larger than 150  $\mu$ m, dispersed oil, with oil droplets in the range of 20–150  $\mu$ m, and emulsified oil, with oil droplets smaller than 20  $\mu$ m. API separators [5] and Dissolved Air Flotation (DAF) devices [6] are used to remove free oil and dispersed oil from wastewater, respectively. They can achieve an efficiency of 98% of oil removal. However, for API separators, the oil droplets need to be relatively large in order to coalesce and DAF separators require the injection of air and addition of PH regulators and coagulants which contribute to the operating cost. More importantly, these conventional methods cannot remove small micron or submicron sized oil droplets. Membrane filtration can be used for removal of emulsified oils and the effluent from industrial operations containing minimal amounts of oil; however, membrane filtration is expensive and requires operating at high pressure.

Several types of sorbents have been studied for the removal of dispersed and emulsified oil from water in packed bed filters or adsorbers. They include activated carbon [7], saw dust [12], organoclay [13], bentonite [14], vermiculite [15], and hydrophobic aquatic plants [16]. Of these materials, only granulated activated carbon (GAC) is commercially used as a sorbent to remove oil and other organics from water [7,17]. However, GAC also displays disadvantages such as slow kinetics and limited removal capacity. Thus, the search for better sorption materials which have high hydrophobicity, high uptake capacity, and high rate of uptake (efficiency) is ongoing.

Hydrophobic silica aerogels have some unique properties; they are highly porous, nanostructured granules that are available as small particles in a variety of different sizes, and because of their hydrophobicity they attract organic molecules and repel water. They consist of tangled, fractal-like chains of spherical clusters of molecules

<sup>\*</sup> Corresponding author. Tel.: + 1 480 9650362. *E-mail address:* robert.pfeffer@asu.edu (R. Pfeffer).

each about 3–4 nm in diameter. The chains form a solid structure surrounding air-filled pores that average about 20 nm. Typical aerogel synthesis is through the sol–gel method, which uses Tetramethoxysilane (TMOS) as the primary precursor. To obtain hydrophobic silica aerogels, Si–OH groups are replaced by hydrolytic stable groups such as Si–R groups ( $R = CH_3$  or  $C_2H_5$  or  $C_3CH_2$ ).

Aerogels are much lighter than water and have the lowest density, and highest surface area per unit volume of any solid. Because of these desirable properties, different types of hydrophobic aerogels have been studied for the sorption of oil and other organics from water [18–21]. It was found that hydrophobic silica aerogels adsorbed miscible and immiscible organic contaminants such as ethanol, toluene, chlorobenzene, trichloroethylene, and others by more than 1–2 orders of magnitude by weight, than activated carbon [18,19] and absorbed as much as 3.5 times its weight of crude oil [20,21]. Recently, Liu et al. [22] showed that hydrophobic silica aerogels exhibited strong adsorption capacity on slightly soluble organic compounds while hydrophilic silica aerogels were much more effective on adsorbing soluble organic compounds from aqueous solution. They also found that the adsorption properties of the silica aerogel remain stable after 5 adsorption/desorption cycles.

When the density of the particulate material (e.g., silica aerogels) is less than the density of the liquid, inverse fluidization can be applied to disperse the solid particles in liquid. Since aerogel granules have a density much lower than water and are robust enough to be fluidized, they can be configured in an inverse fluidized bed, where the oilcontaminated water flows downward through a distributor and through the bed of particles. One of the key works for the hydrodynamic characterization of liquid phase fluidization is that of Richardson and Zaki [23], published in 1954, and still applicable today. They found that the settling velocity of the particles or the superficial velocity of a liquid in a fluidized bed divided by the terminal velocity of a single particle is an exponential function of the void fraction in the bed. Since then, many studies of the hydrodynamic characteristics and bed expansion of liquid-solid and liquid-solid-gas inverse fluidization have been reported in the literature [24-33]. The benefits of using inverse fluidization as compared to a more simple packed bed of particles are a low and constant pressure drop when operating above the minimum fluidization velocity, excellent mixing between the solid particles and the liquid (approaching CSTR conditions), high heat and mass transfer rate, an adjustable voidage of the fluidized bed by changing the fluid velocity, and the ability for continuous operation.

A recent paper by Quevedo et al. [34] used an inverse fluidized bed of hydrophobic silica aerogels to remove vegetable oil from water. Using a diaphragm pump, they added a small quantity of pure oil to a flowing water stream, the oil–water mixture was then passed through a static mixer made up of steel wire packing to disperse the oil into the water; however, the oil droplets entering the fluidized bed were greater than 20 µm (dispersed oil). They found that an inlet oil concentration of about 1000 mg/L could be reduced to less than 100 mg/L by this method before a significant amount of aerogels became loaded with oil and left the bed at the bottom of the column.

The objectives of the work reported in this paper are to measure some of the physical properties of the hydrophobic silica aerogels (Nanogel®) provided to us by Cabot Corporation, study the hydrodynamics characteristics of the Nanogel granules in the inverse fluidized bed, and determine the feasibility of using Nanogel granules for removing emulsified oil (droplets less than 20 µm) from stable oil-inwater emulsions using inverse fluidization. Cabot Nanogel is covered with Tri–Methyl–Silyl–groups (TMS) so that its surface is hydrophobic.

## 2. Experimental equipment and methods

# 2.1. Materials

The following materials were used in our experimental work: Nanogel of different size ranges, 0.5–0.85 mm (sieved TLD 101), 0.7–

1.2 mm (TLD 301), and 1.7–2.35 mm (sieved TLD 302) was supplied by Cabot Corporation. The contact angles of the hydrophobic Nanogel, as reported by Cabot Corporation, are between 160° and 170°. Using a goniometer in our laboratory, we measured lower contact angles between 130° and 140°. Supermarket vegetable oil (Food Club) stabilized by the surfactant Tween 80 (Aldrich) was mixed with deionized water for the inverse fluidized bed experiments.

## 2.2. Surface and pore size analysis

The pore structure (BET surface area, pore size distribution, and pore diameter) of the three size ranges of Nanogel were measured by nitrogen adsorption porosimetry (Micromeritics 2020). Each run was performed using approximately 0.15 g of sample which was pretreated at 120 °C under vacuum at 1.5 Pa.

#### 2.3. Nanogel density measurement

It is difficult to measure the granule density of the Nanogel by using a traditional method such as a liquid pycnometer. This is because the inter-particle forces between the aerogels agglomerate small particles so strongly, that it is difficult to open all the voids around the particles in order to replace the air/gas with a liquid. Hence Cabot Corporation lists the bulk density and the internal porosity of the Nanogel granules to be about 64 kg/m³ and 0.95, respectively, on their website but only gives a rough estimate of the value of the granule density. In this paper, the granule density of the Nanogels was measured by an inverse fluidization method, i.e., the pressure drop after the bed was fully fluidized (in the pressure plateau region) was measured and used to calculate the granule density.

# 2.4. Inverse fluidized bed experiments for measuring hydrodynamic characteristics

A schematic diagram of the experimental setup used for inverse fluidization of Nanogel granules by water is shown in Fig. 1. It consists of a fluidization column, valves and piping, flow meters, a metering pump, static mixers, pressure gauge and a differential pressure transmitter with a display. The fluidization column was made of PVC with an internal diameter (ID) of 0.076 m (3 in.) and an outer diameter (OD) of 0.089 m (3.5 in.). Two different column lengths were used: 1.47 m (58 in.) and 0.77 m (30 in.). The valves and piping were also made of PVC, and the pipe size was 1 in. The flow of deionized water was adjusted by ball valves, and flow readings were taken by two calibrated electronic digital flow meters, one for the range between 0 and 3 GPM and the other for the range between 3 and 50 GPM (GPI series A109). The metering pump (Pulsatron series A Plus, 0–6 GPD) and three static mixers (placed in series in the piping after the pump inlet) were used to study the efficiency and removal capacity of emulsified oil in the fluidized bed of Nanogels. Only clean deionized water was used in the hydrodynamics experiments.

A typical experimental run is described as follows. First, the pressure drop across the empty column was measured at different water flow rates in order to obtain a correlation that can be used to determine the pressure drop of the fluidized bed alone; this was done by subtracting the empty column pressure drop from the total fluidized bed pressure drop. Then the particles to be fluidized were loaded into the fluidization column. Next, the column was filled with water from the bottom and air was completely removed by a vent at a high point in the system. Then the water flow was fed at the top of the column through a distributor made up of a packed bed of glass beads supported by a steel wire mesh to prevent channeling. The Nanogel was inversely fluidized by increasing the flow until the drag force on the particles balances the buoyant force less the gravity force (minimum fluidization velocity). The flow rate was then increased significantly above that value and the hydrodynamic parameters, bed

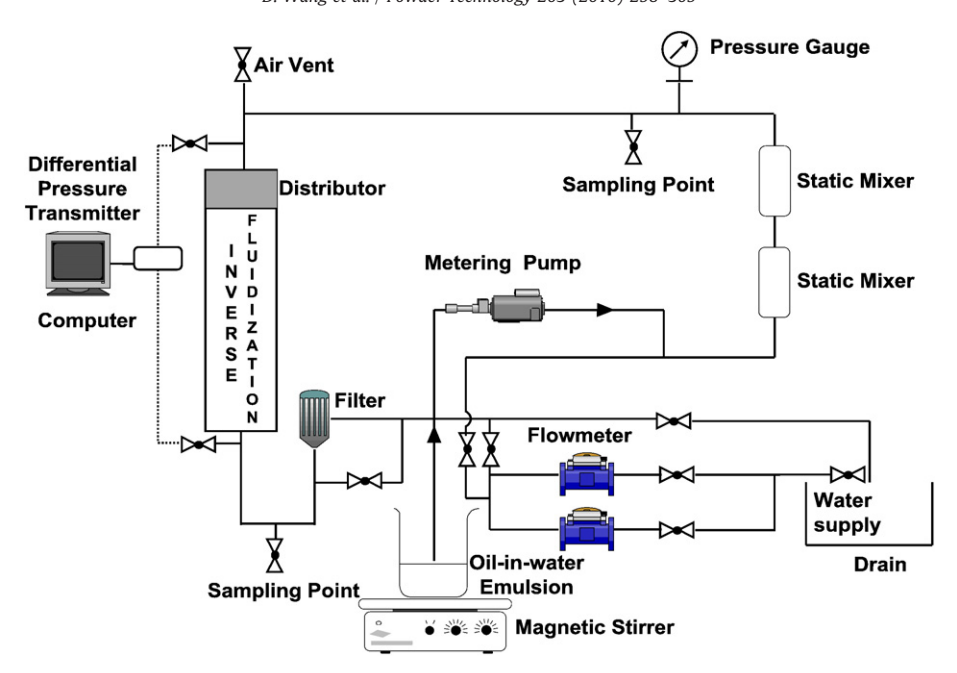


Fig. 1. Schematic diagram of the inverse fluidization experimental setup.

height and pressure drop were measured at each flow rate by gradually decreasing the flow of water until the bed defluidizes (packed bed condition) and then increasing the flow again until the bed height had expanded by at least a factor of two. The static pressure before the column was kept constant to ensure consistent readings.

## 2.5. Inverse fluidized bed experiments for oil removal

The concentration of oil in water was measured by analyzing chemical oxygen demand (COD) in the sample. Since oil was the dominating organic substance added to the water, it was reasonable to assume that any increase in COD levels was due to the addition of oil. COD was measured by using a HACH DR/890 colorimeter following the procedure indicated in the HACH manual, in particular, Method 8000: reactor digestion method USEPA approved for COD [35,36].

In the inverse fluidized bed experiments to measure the oil removal efficiency and capacity, a constant deionized water superficial velocity above the minimum fluidization velocity and a constant static pressure was maintained throughout the duration of the experiment. A high-concentration, stable oil-in-water emulsion was continuously stirred by a magnetic stirrer in a large plastic container and was injected into the piping system by the pump upstream of the static mixers and the fluidization column. By adjusting the pump's stoke displacement and frequency, a desired concentration of oil (1000 ppm COD or less) was obtained when the emulsion was mixed into the flowing water. Samples of water of about 250 ml, upstream and downstream of the inverse fluidized bed, were taken at regular intervals for COD concentration analysis until the expanded bed height reached the bottom of the column and some Nanogel was observed to leave the bed with the water.

Since the oil present in waste water is usually in an emulsified form (oil droplets smaller than 20  $\mu m$ ), we wanted to add a stable oil-in-water emulsion rather than adding pure oil droplets into the inverse fluidized bed as was done by Quevedo et al. [34]. The oil-in-water emulsion was prepared by adding a small amount of the surfactant Tween 80, about 1 to 4 volume % of the amount of oil added to the water to form the emulsion and the mixture was mixed in a blender for a few minutes. Then, the emulsion was kept stirred by using a magnetic stirrer to keep it stable during the inverse fluidized bed experiment. The size of the oil droplets in the oil-in-water

emulsions was measured by using an optical microscope. The stability of the oil-in-water emulsion was measured by sending the emulsion through the empty column (without any Nanogel present) and comparing the difference between the average value of the inlet and outlet oil concentration.

# 2.6. Batch equilibrium measurements for oil-in-water emulsion

To measure the adsorption isotherm of the Nanogels, six representative weights of TLD 301 Nanogel, in the range of 20–400 mg, were mixed with 100 mL of around 1000 ppm COD oil-inwater emulsions (using 4% Tween 80) in glass bottles. These bottles were shaken in an Innova 4080 incubator shaker (200 rpm) at room temperature. Upon reaching equilibrium (>3 h), all the samples were withdrawn and analyzed by the HACH DR/890 colorimeter.

## 2.7. Batch kinetic measurements for oil-in-water emulsion

Batch kinetic experiments were conducted at room temperature. A number of glass bottles containing 100 mL of around 1000 ppm COD oil-in-water emulsions were mixed with 100 mg of TLD 301 Nanogel in the Innova shaker at 200 rpm for different time periods. The concentration of each of the liquid samples was measured by the HACH DR/890 colorimeter.

# 3. Theoretical model

Although some modeling of the adsorption behavior in a liquid-solid fluidized bed has been reported in the literature [37–39], we would like to compare our inverse fluidized bed experimental results with a model that is based on the equilibrium and kinetic data for our particular Nanogel-oil-in-water emulsion system. As will be shown below, the breakthrough curves in our inverse fluidized bed absorber are considerably different than those expected in a comparable fixed bed adsorber. This is due to the considerable axial mixing occurring in the solid and liquid phases, especially when the inverse fluidized bed height is relatively short. In order to describe the emulsified oil adsorption in the inverse fluidized bed, a model was developed taking into account hydrodynamic behavior, dispersion, and mass transfer between the liquid and solid phases.

# 3.1. Model development

The governing equations of the model were derived based on the assumptions listed below: (1) Nanogel particles are monosize and the average particle size is used; (2) radial concentration gradients are negligible for both the liquid and solid phases in the column; (3) rate of adsorption is determined by the linear driving force model (see below) based on the batch kinetic data; (4) adsorption equilibrium is represented by Freundlich equation; (5) the solid phase is completely mixed (short fluidized bed height) and the liquid phase is described by an axial dispersion model; and (6) bed height is expressed as the function of time based on the experimental data.

# 3.2. Derivation of model equations

Following Veeraraghavan and Fan [37], the mass balance with respect to the adsorbate in the liquid phase gives

$$\varepsilon \frac{\partial C}{\partial t} = D_{ax} \varepsilon \frac{\partial^2 C}{\partial z^2} - u \frac{\partial C}{\partial z} - (1 - \varepsilon) K'(C - C_e)$$
 (1)

where  $\varepsilon$  the void fraction of the fluidized bed, C is the oil concentration in the liquid phase in the fluidized bed,  $C_{\rm e}$  is the local equilibrium concentration in the liquid phase corresponding to the adsorbate concentration at the Nanogel particle boundary,  $D_{\rm ax}$  is the liquid phase axial dispersion coefficient, u is the superficial fluid velocity, and K' is the adsorption rate constant.

The initial and boundary conditions for the inverse fluidized bed subject to a switch in the feed from the pure water stream to an oil-inwater emulsion stream are

$$t = 0, \quad C(z, 0) = 0, \quad 0 \le z \le H$$
 (1a)

$$z = 0, \quad C = C_0 + \frac{D_{ax}\varepsilon}{u} \frac{\partial C}{\partial z}, \quad t > 0$$
 (1b)

$$z = H$$
,  $\frac{\partial C}{\partial z} = 0$ ,  $t > 0$ , (where  $H$  is a function of  $t$ ) (1c)

where H is the height of the fluidized bed and  $C_0$  is the oil-in-water feed concentration.

The liquid phase axial dispersion coefficient,  $D_{ax}$  is calculated using an equation presented by Chung and Wen [40]

$$\frac{D_{ax}\rho_l}{\mu} = \frac{\textit{Re}}{0.2 + 0.011\textit{Re}^{0.48}} \tag{2}$$

where  $\rho_{\rm l}$  is the density of fluid,  $\mu$  is the fluid viscosity, and  ${\it Re}$  is Reynolds number.

There is no convective flow in the solid phase and, in addition, we assume that the solid phase is completely mixed. Hence

$$H\frac{\partial q}{\partial t} = \int_0^H \frac{K'}{\Omega_{\rm p}} (C - C_{\rm e}) dz \tag{3}$$

where  $\rho_{\rm P}$  is the density of the particle, and q is the mass of oil per unit mass of Nanogel in the particle.

The initial condition is

$$t = 0, \quad q(0) = 0, \quad 0 \le z \le H$$
 (3a)

Finally, the Freundlich equation, defined as

$$q = kC_e^{1/n} \tag{4}$$

where k and n are the Freundlich equilibrium constants, is used to relate the amount of oil adsorbed per weight of Nanogel to the concentration of oil in the liquid phase at equilibrium.

The rate constant *K'* in Eqs. (1) and (3) is obtained from the batch kinetic experiment by using a linear driving force model defined as

$$V_{\rm I}\frac{dC'}{dt} = -\frac{m}{\rho_{\rm P}}K'(C' - C'_{\rm e}) \tag{5}$$

$$V_{l}\frac{dC'}{dt} = -m\frac{dq'}{dt} \tag{6}$$

with initial condition

$$t = 0, \quad C'(0) = C'_0$$
 (5a)

where  $V_1$  is the liquid volume, m is the mass of Nanogels, C' is the oil concentration in the liquid phase,  $C'_e$  is the local equilibrium concentration in the liquid phase corresponding to the adsorbate concentration at the Nanogel particle boundary,  $C'_0$  is the initial oil concentration and q' is the mass of oil per unit mass of Nanogel in the particle.

Eqs. (4), (5) and (6) can be solved simultaneously to obtain values of C' at different times by assuming a value of K'. The actual value of K' can then be obtained by comparing the calculated values of C' with the experimentally measured values of C' using a least squares regression.

#### 3.3. Simulation

The governing Eqs. (1) and (3) are nonlinear partial differential equations. In these equations, C is a function of t and z, and q is only a function of t because of the assumption that the solid phase is well mixed. The spatial discretization method was used to transform these partial differential equations into a set of ordinary differential equations: these equations were discretized in space using finite differences with 50 evenly spaced finite difference points along the column length. This set of ordinary differential equations was solved using a Runge-Kutta 23 simulation method programmed in Matlab R2008b, the step size in the program was approximately 0.05-0.1 s.

### 4. Results and discussion

# 4.1. Pore structure of Nanogels

N<sub>2</sub> adsorption—desorption isotherms for the three different Nanogel size range samples were found to be almost identical and show a type IV isotherm which corresponds to a mesoporous material. The three different particle sized Nanogel also have a similar pore size distribution and the most prevalent pore size is about 15 nm. Specific surface area and pore diameter of the different particle size Nanogel are shown in Table 1; the pore volume measurements are inaccurate because of the presence of macropores and are therefore not included in the table. From these results we conclude that the three Nanogel samples of different size ranges have similar pore structures and very high specific surface.

# 4.2. Hydrodynamics of inverse fluidized beds of Nanogel granules

The hydrodynamic characteristics of inverse fluidized beds of Nanogel granules are represented by the fluidized bed pressure drop

**Table 1**Specific surface area and pore diameter results for three different particle size range Nanogel.

Sample	Particle sizes	Surface properties	Surface properties			
		Specific surface (m <sup>2</sup> /g)	Average pore size (nm)			
TLD 101	0.5-0.85 mm	660	15.2			
TLD 301	0.7-1.2 mm	686	15.7			
TLD 302	1.7-2.35 mm	671	15.6			

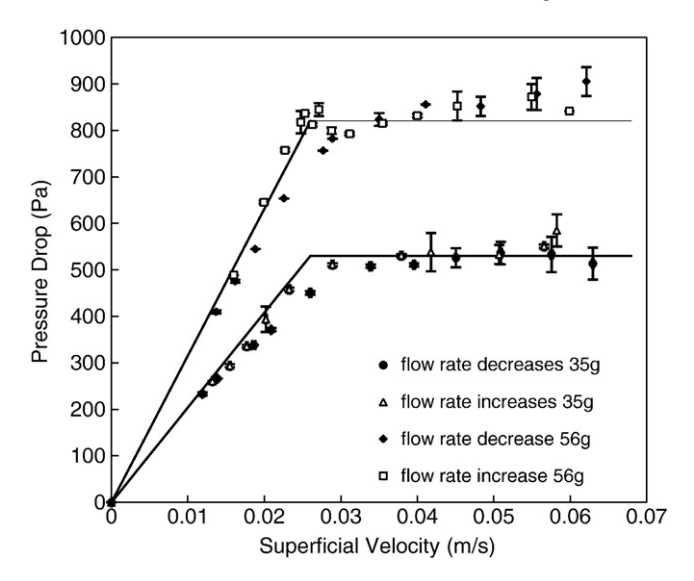
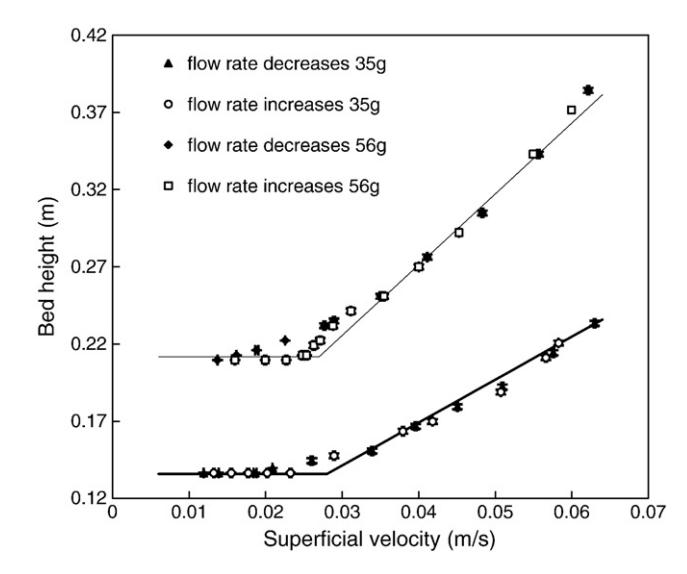


**Fig. 2.** Inverse fluidized bed pressure drop vs. superficial fluid velocity of TLD 302, 1.7–2.35 mm Nanogel granules.

and the bed expansion. Fig. 2 shows the fluidized bed pressure drop plotted against the superficial fluid velocity for TLD 302, 1.7–2.35 mm Nanogel granules. This plot is used to estimate the minimum fluidization velocity, i.e., the velocity where the particle configuration changes from a packed bed to a fluidized bed and the pressure drop becomes constant. Fig. 3 shows the fluidized bed height as a function of superficial velocity corresponding to Fig. 2. These two figures show that: (1) the pressure drop rises linearly below minimum fluidization in the packed bed region and then plateaus above minimum fluidization, and (2) the bed height remains relatively constant before minimum fluidization and then expands as the water velocity is increased above minimum fluidization. Table 2 shows the minimum fluidization velocity and plateau pressure drop of the three different particle size range Nanogel. As seen in the table, the minimum fluidization velocity is dependent on the granule size and is independent of the amount of the granules fluidized. The larger the granule size, the higher the minimum fluidization velocity.



 $\textbf{Fig. 3.} \ \text{Inverse fluidized bed height vs. superficial fluid velocity of TLD 302, 1.7-2.35 mm Nanogel granules. } \\$ 

**Table 2**Minimum fluidization velocity and plateau pressure drop results for three different particle size ranges Nanogel in the inverse fluidized bed.

Particle sizes/type (mm/type)	Mass (g)	$\triangle P$ (Pa)	$U_{\rm mf}$ (m/s)
0.5-0.85 TLD 101	56	$876 \pm 64$	0.015
	70	$1046 \pm 53$	
0.7-1.2 TLD 301	35	$492 \pm 15$	0.017
	70	$988 \pm 32$	
1.7-2.35 TLD 302	35	$536 \pm 21$	0.026
	56	$853 \pm 27$	
	70	$1108 \pm 36$	

## 4.3. Density and the external porosity of the granules

The value of the granule density can be calculated from the experimental data by using a force balance. The fluidized granules are acted on by a buoyancy force ( $F_{\rm B}$ ), gravity force ( $F_{\rm g}$ ) and drag force ( $F_{\rm D}$ ). The buoyancy and gravity forces are

$$F_{\rm B} = \rho_{\rm I} V_{\rm P} g$$
 and  $F_{\rm g} = \rho_{\rm p} V_{\rm P} g$  (7)

where  $V_P$  is the total volume of particles fluidized in the column. The drag force applied on the particles during fluidization (assuming negligible wall effects) is given by the experimental pressure drop  $(\Delta P_{\rm exp})$  multiplied by the cross sectional area of the fluidization column (A)

$$F_{\rm D} = \Delta P_{\rm exp} A \tag{8}$$

A force balance on the particle gives

$$F_{\rm B} = F_{\rm g} + F_{\rm D} = \rho_{\rm P} V_{\rm P} g + \Delta P_{\rm exp} A = \rho_{\rm I} V_{\rm P} g \tag{9}$$

Since  $m_p = \rho_p V_p$ , Eq. (9) can be written as

$$V_{\rm p} = \frac{\left(\Delta P_{\rm exp} A + m_{\rm p} g\right)}{\rho_{\rm l} g} \tag{10}$$

and the granule density of the particles is given by  $\rho_P = \frac{m_P}{V_P}$  with  $V_P$  obtained from Eq. (10). The void volume can be found by subtracting the volume of the particles  $(V_P)$  from the total volume of the fluidized bed  $(V_b)$ . Hence, the void fraction of the fluidized bed is

$$\epsilon = \frac{V_{\epsilon}}{V_{b}} = \frac{V_{b} - V_{p}}{V_{b}} = 1 - \frac{V_{p}}{V_{b}} = 1 - \frac{m_{p}}{\rho_{p}V_{b}} = 1 - \frac{m_{p}}{\rho_{p}AH} \tag{11}$$

Eq. (10) is of the particular significance since it can be used to calculate the particle density if the pressures drop measurement is reliable. It can also be used to predict the pressure drop across the fluidized bed if the particle density is known. The Nanogel density and initial void fraction are calculated and listed in Table 3. As seen in the

**Table 3**Nanogel density and initial void fraction calculation results from experiment data.

Particle size	Mass (g)	<i>V</i> <sub>P</sub> (m <sup>3</sup> )	$ ho_{ m P}$ (kg/m <sup>3</sup> )	Initial bed height (m)	Bulk density (kg/m³)	Initial void fraction
0.5-0.85 mm	56	$(4.6 \pm 0.3)E - 04$	$121\pm8$	0.27	46	0.63
	70	$(5.6 \pm 0.2)E - 04$	$126 \pm 6$	0.32	48	0.62
0.7-1.2 mm	35	$(2.6 \pm 0.1)E - 04$	$131 \pm 4$	0.15	51	0.62
	70	$(5.3 \pm 0.1)E - 04$	$133 \pm 4$	0.29	53	0.60
1.7-2.36 mm	35	$(3.1 \pm 0.1)E - 04$	$123 \pm 4$	0.14	55	0.51
	56	$(4.5 \pm 0.1)E - 04$	$123 \pm 3$	0.21	59	0.53
	70	$(6.0 \pm 0.2)E - 04$	$120\pm3$	0.27	57	0.51

table, the densities of the three different size ranges of Nanogel vary between  $120 \text{ kg/m}^3$  and  $133 \text{ kg/m}^3$ , and the average granule density of the Nanogel particles is  $125 \pm 5 \text{ kg/m}^3$ .

## 4.4. Mathematical models of bed expansion

The Richardson–Zaki (R–Z) correlation [23] is among the most useful methods to describe the relationship between the void fraction and superficial velocity in a conventional liquid fluidized bed. The R–Z equation is

$$\varepsilon^n = \frac{U}{U_i} \tag{12}$$

where U is the superficial velocity and  $U_i$  is the settling velocity of a particle at infinite dilution. The R–Z exponent or index (n) is a function of the particle terminal Reynolds number  $(Re_t)$ . For the TLD 302 (1.7-2.35 mm) Nanogels

$$n = 4.45Re_{\rm t}^{-0.1}$$
 for  $200 < Re_{\rm t} < 500$  (13)

Where 
$$Re_{\rm t} = \frac{U_{\rm t}\rho_{\rm t}d_{\rm P}}{\mu_{\rm t}}$$
 (14)

The settling velocity at infinite dilution  $(U_i)$  and the terminal velocity  $(U_t)$  are related by

$$\log (U_{\rm i}) = \log U_{\rm t} - \frac{d_{\rm P}}{D} \tag{15}$$

The R–Z exponent (n) can also be obtained from the experimental data by plotting the logarithm of the superficial velocity against the logarithm of the void fraction

$$ln U = n ln (\varepsilon) + ln (U_i)$$
(16)

After calculating the void fraction ( $\varepsilon$ ) from Eq. (11), the experimental data are plotted in Fig. 4 for three different amounts of fluidized TLD 302, 1.7–2.35 mm Nanogel granules and using our experimental data and the equations above, the Richardson–Zaki exponent (n), and the terminal velocity ( $U_{\rm t}$ ) were calculated and shown in Table 4. As seen in the table, the values of the Richardson–

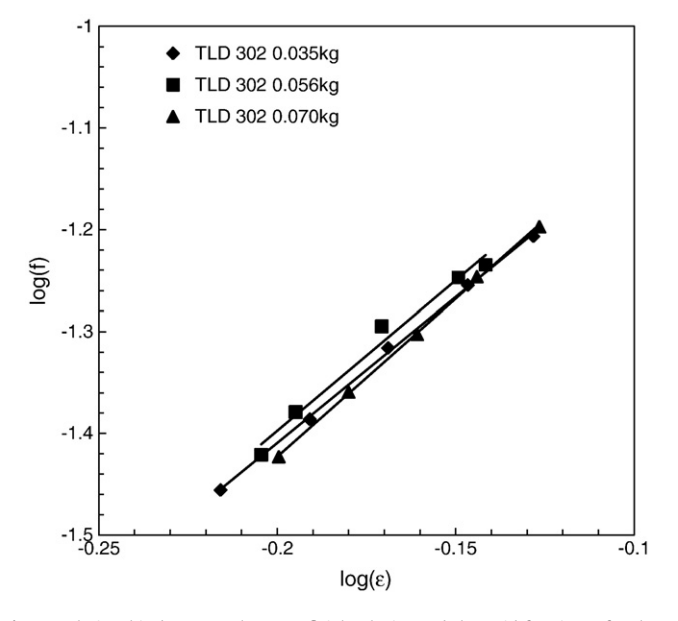


**Fig. 4.** Relationship between the superficial velocity and the void fraction  $\varepsilon$  for three different amounts of TLD 302 Nanogels accordingly to the R–Z equation.

**Table 4**Richardson–Zaki bed expansion parameters for 35 g, 56 g and 70 g TLD 302 Nanogel particles from the experiment data and calculated using Eqs. (13–15).

Mass (g)	R-Z (exp) (n)	R-Z (exp) ( <i>U</i> <sub>i</sub> ) (m/s)	U <sub>t</sub> Eq. (15) (m/s)	Re <sub>t</sub> Eq. (13)	R–Z Eq. (13) (n)
35	2.87	0.145	0.154	310	2.52
56	2.95	0.155	0.164	333	2.49
70	3.10	0.158	0.169	340	2.48

Zaki exponent (n), for 1.7–2.35 mm nanogel granules, calculated from Eq. (13) are somewhat lower than the experimental values. This may possibly be due to the fact that the data were obtained in an inverse fluidized bed rather than a conventional fluidized bed.

There are very few correlations for an inverse fluidized bed, though several models are available for correlating bed expansion with fluid superficial velocity in a conventional liquid-solid fluidized bed (such as the R–Z model above). Fan et al. [24] proposed a model based on a drag force function, f, which can be used to describe the bed expansion in an inverse fluidized bed. This correlation expressed in terms of the void fraction of the inverse fluidized bed  $\varepsilon$ , Archimedes number  $Ar = d^3_{\ p}(\rho_1 - \rho_p)\rho_1 g/\mu^2_1$ , Reynolds number  $Re = \frac{U\rho_1 d_p}{\mu_1}$  and the ratio of the particle size to the bed diameter is

$$f = 3.21 \varepsilon^{-4.05} A r^{-0.07} \exp\left(3.5 \frac{d_{\rm P}}{D}\right) \tag{17}$$

In this model, a drag force function, *f*, defined as the ratio of the drag force of fluid on particles in a multiparticle system to that in a single particle system, is a function of the Archimedes number and the Reynolds number. This drag force function for the inverse fluidization system taken from Fan et al. [24] is

$$f = \frac{Ar}{13.9Re^{1.4}} \qquad \text{for } 2 < Re < 500$$
 (18)

$$f = \frac{3Ar}{Re^2} \qquad \text{for } Re > 500 \tag{19}$$

where the Archimedes number and the Reynolds number at different flow superficial velocities can be calculated from the experimental data. The void fraction of the inverse fluidized bed  $\varepsilon$  at different flow superficial velocities can be calculated from Eq. (11).

By plotting the logarithm of the drag force function f against the logarithm of the void fraction  $\varepsilon$ , the slope of the straight line (see Eq. (17)) can be obtained, which should be close to -4.05 according to Fan et al. [24]. After calculating the void fraction ( $\varepsilon$ ) from Eq. (11) and the drag force function f from Eq. (18), the experimental data are plotted in Fig. 5 for 35 g of TLD 301 0.7–1.2 mm Nanogel granules and three different amounts of TLD 302 1.7–2.35 mm Nanogel granules. As seen in the figure, straight lines are obtained for all these four experimental runs; the slope of -4.04 for TLD-301 nanogels and the average slope of -4.15 for TLD 302 Nanogels closely agree with the value of -4.05 suggested by Fan et al. [24].

4.5. Removal of oil from water in an inverse fluidized bed and an inverse packed–fluidized bed of Nanogel granules

Fig. 6(a) and (b) shows the size of the oil droplets in oil-in-water emulsions with 1% and 4% Tween 80 added. As seen in this figure, the size of most of the oil droplets is less than 20  $\mu m$ , which indicates that the oil droplets produced in our experiments can be classified as emulsified oil. Without adding the Tween 80 stabilizer, the oil droplets are much larger than 20  $\mu m$  (see Fig. 6(c)) indicating the presence of dispersed oil.

Table 5 shows the emulsion stability experiment results. The addition of 4% by volume (or higher) of Tween 80 as compared to the

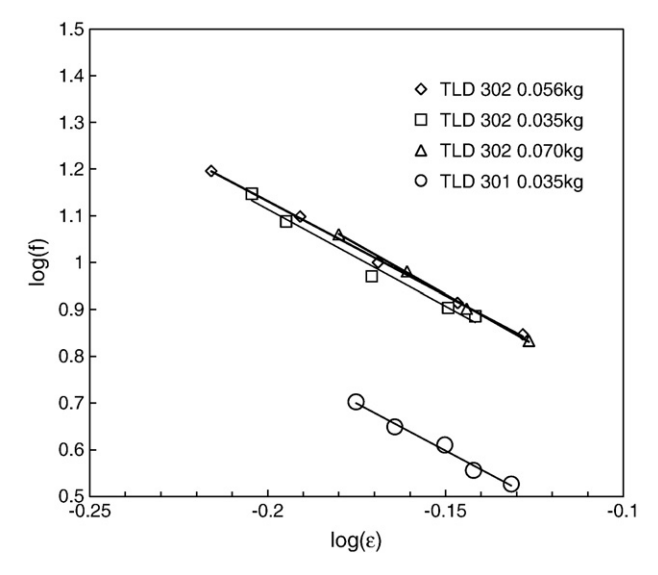


**Fig. 5.** Relationship between the drag force 'f' as defined by Fan et al. [24] and the void fraction  $\varepsilon$  for TLD 301, 0.7–1.2 mm and TLD 302 sieved, 1.7–2.35 mm.

amount of oil added produces an emulsion that remains stable without stirring for 1 h. That is, the average inlet concentration (COD) (after being mixed with deionized water) measured at 10 min intervals differed from the average outlet concentration by less than 5% when passed through the empty column (without Nanogel present). Before starting an inverse fluidized bed experiment, the Tween 80 stabilized oil-in-water emulsion is mixed in a blender for a few minutes and the emulsion is kept stirred with a magnetic stirrer to keep it stable during the duration of the experiment.

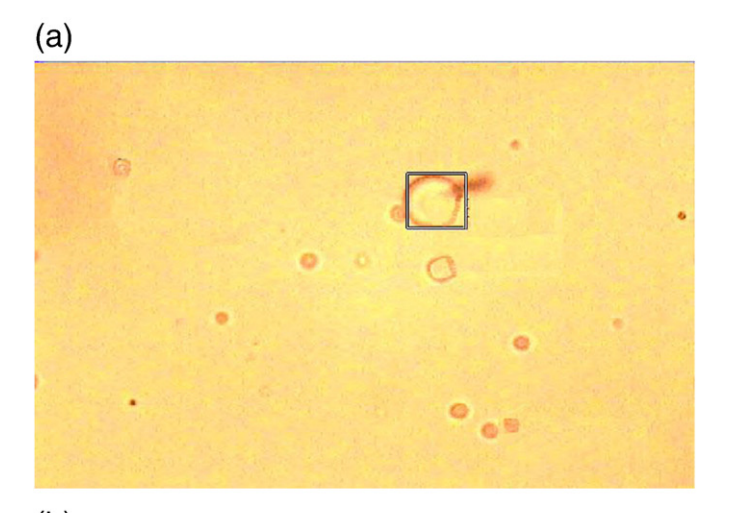
The oil removal efficiency and capacity of the Nanogel granules are studied by measuring both the inlet and exit concentrations of oil as a function of time and plotting a breakthrough curve. Ideally, the inlet oil concentration should remain constant throughout the experiment, but small changes in the water pressure, oil pump flow rate and stability of the emulsion result in somewhat different inlet concentrations with time; hence an average value is used. From the breakthrough curve, the amount of oil removed by the inverse fluidization process is given by

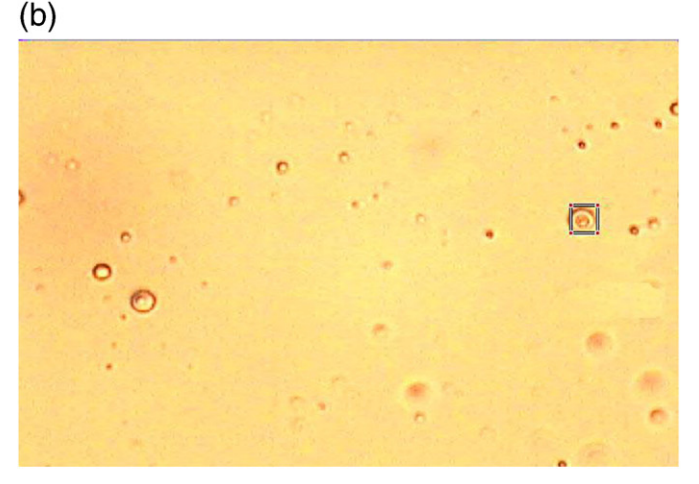
$$m_{\text{Removal}} = F \overline{C_{\text{in}}} t - F \int_{0}^{t} C_{\text{out}} dt$$
 (20)

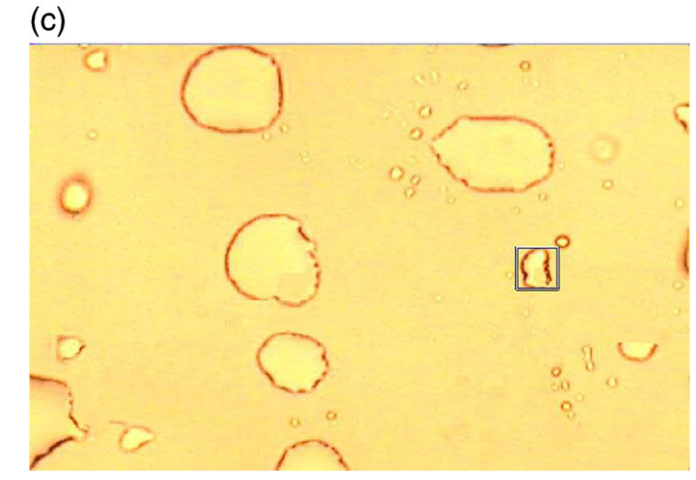
where  $m_{\rm Removal}$  is the weight of oil removed by the aerogel granules, F is the flow rate during the experiment,  $\overline{C_{\rm in}}$  is the average inlet oil concentration,  $C_{\rm out}$  is the outlet oil concentration, t is the time when the fluidized bed is no longer stable and Nanogel granules begin to leave the column due to their decrease in buoyancy as they adsorb/absorb oil.

The inlet and outlet concentrations of oil are monitored by analyzing the chemical oxygen demand (COD) at several time intervals during the experiments. A calibration curve relating the measured COD concentration to the actual oil concentration in mg/l is shown in Fig. 7.

The breakthrough curve in each experimental run is obtained from the experiment concentration versus time data. Table 6 shows the operating conditions for each experiment. The following parameters are changed to compare the oil removal efficiency: the proportion of Tween 80 in the oil-in-water emulsion, fluid superficial velocity, particle (granule) size range, and amount of particles. The breakthrough curves under different operating conditions are shown in Figs. 8–10 for inverse fluidization and Fig. 11 for an inverse packed-fluidized bed. Here we have started the experiment at a flow rate (water velocity) which is below the minimum fluidization velocity so that the bed remains in the packed bed mode until the Nanogel



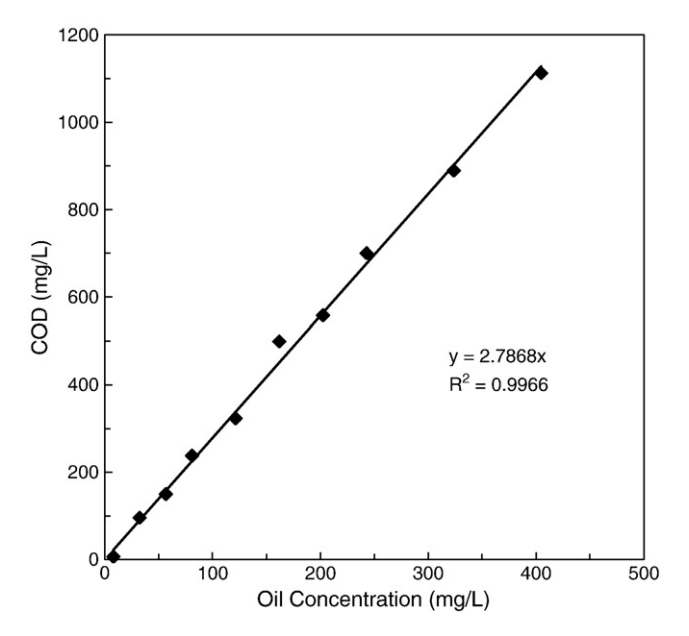


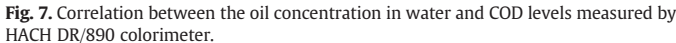


**Fig. 6.** Marked oil droplet size with different amounts of Tween 80: (a) 1% Tween 80, height 12.4  $\mu$ m, width 11.9  $\mu$ m, in the range of emulsified oil, (b) 4% Tween 80, height 5.7  $\mu$ m, width 5.8  $\mu$ m, in the range of emulsified oil, and (c) 0% Tween 80, height 95.6  $\mu$ m, width 83.5  $\mu$ m, in the range of dispersed oil.

**Table 5**Oil-in-water emulsion stability results for different proportions of emulsifier (Tween 80).

Proportion of Tween 80	0.5%	1%	3%	4%	5%
Inlet average COD concentration (mg/L)	1092	1091	1065	1085	1104
Outlet average COD concentration (mg/L)	687	966	978	1058	1065
Decrease	37%	11%	8.2%	2.3%	3.6%





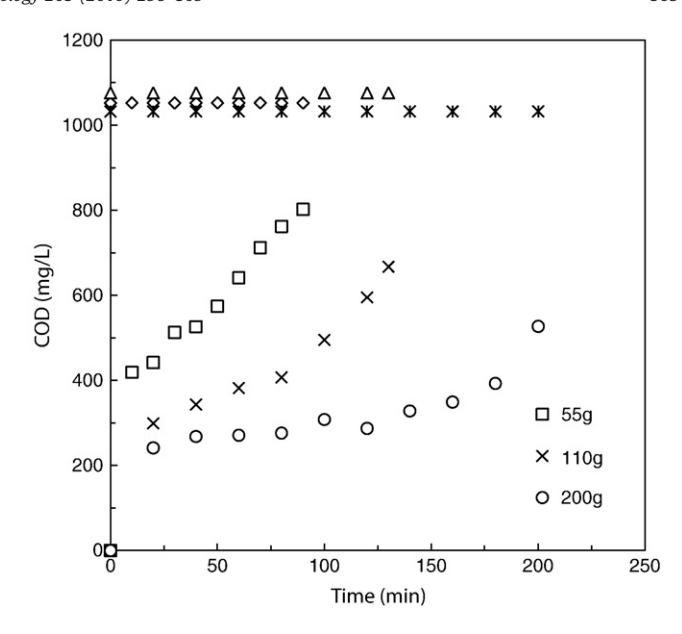


**Fig. 8.** Breakthrough curve in fluidized bed for 55 g, 110 g and 200 g TLD 301, 0.7–1.2 mm Nanogel granules when the proportion of Tween 80 is 4%, the inlet COD is around 1000 mg/L and  $U/U_{\rm mf}$  is 1.1.

granules adsorb/absorb sufficient oil to decrease the net buoyancy force (buoyancy minus gravity) acting on them and the bed fluidizes.

We also started a run using an emulsion stabilized by 1% Tween 80 as a fluidized bed ( $U/U_{\rm mf}=1.1$ ) and when the bed expanded, but before any Nanogels left the column, we decreased the flow rate below minimum fluidization ( $U/U_{\rm mf}=0.67$ ) and ran as a packed bed. This allowed us to continue the experiment without losing Nanogel granules from the bottom of the column. The breakthrough curve for this experimental run is shown in Fig. 12.

The removal capacity (kg oil/kg Nanogel) using Eq. (20) based on the breakthrough curves is also shown in Table 6 and varied between 1.2 to 1.84 for the fluidized bed and 2.26–2.77 for the packed-fluidized bed mode when the proportion of Tween 80 in the emulsion is 4% and varied between 1.51 and 2.13 for the fluidized bed when Tween 80 in emulsion is reduced to 1%.

The shape and sharpness of the breakthrough curve for a given adsorbent mainly depend on such factors as the adsorption isotherm at equilibrium, the mass transfer rate, and hydrodynamic factors such as bed height and contact (residence) time. As already mentioned, the breakthrough time in a fluidized bed adsorber is considerably shorter than in a fixed bed adsorber due to the large axial mixing in the fluidized bed. In our experiments, the outlet oil concentrations in the

beginning of the experiment are high and the oil removal efficiencies are relatively low. There are several possible reasons for these results: (1) the contact time through the fluidized bed or packed-fluidized bed is too short (less than 1 min) and is not long enough for the Nanogels to absorb the oil passing through them and (2) while the presence of the emulsifier, Tween 80, greatly increases the stability of the oil-in-water emulsion, it may also hinder the adsorption/ absorption of oil by the Nanogel surfaces. According to Hrubesh et al. [18], solvents that are insoluble in water are separated by selectively wetting the surfaces of the aerogels, entering the pores and subsequently absorbed into the porous structure. Even though very little Tween 80 is present (only 1% or 4% of the volume of oil in the emulsion), since the surfactant can physically interact with both oil and water, the hydrophilic end of the Tween 80 may allow some water molecules to attach to the surface and enter the nanogel particles thus reducing the Nanogel adsorption/absorption capacity

To check whether the Tween 80 has an effect on the adsorption/ absorption capacity of the Nanogels, we also did runs using only 1% of Tween, as seen in Figs. 9 and 12. If we compare Figs. 8 and 9 for TLD 301 Nanogel, Fig. 8 shows outlet concentrations at short times that are almost twice as large as the outlet concentrations at short times in

**Table 6**Summary of experimental conditions and oil removal capacity from water by an inverse fluidized bed, packed–fluidized bed or fluidized–packed bed of Nanogel.

Nanogel type	Particle size (mm)	Figure #	% Tween 80	Nanogel mass (g)	Flow rate (GPM)	U/U <sub>mf</sub> ratio	Entrance COD (mg/L) (average)	Removal capacity (kg oil / kg Nanogel)
TLD 301	0.7-1.2	8	4%	55	1.3	1.1	$1052 \pm 30$	1.43
TLD 301	0.7-1.2	8	4%	110	1.3	1.1	$1076 \pm 67$	1.35
TLD 301	0.7-1.2	8	4%	200	1.3	1.1	1032±49	1.26
TLD 301	0.7-1.2	9	1%	55	1.3	1.1	$1094 \pm 51$	2.13
TLD 301	0.7-1.2	9	1%	110	1.3	1.1	$1075 \pm 81$	1.75
TLD 301	0.7-1.2	9	1%	200	1.3	1.1	$1163 \pm 102$	1.51
TLD 302	1.7-2.3	10	4%	110	2.0	1.1	$1104 \pm 51$	1.84
TLD 302	1.7-2.3	11	4%	55	1.2	0.67	$1198 \pm 118$	2.26 <sup>a</sup>
TLD 302	1.7-2.3	11	4%	55	1.0	0.56	$1211 \pm 51$	2.77 <sup>a</sup>
TLD 302	1.7-2.3	12	1%	110	2.0-1.2	1.1-0.67	$1007\pm32$	1.91 <sup>b</sup>

a Packed-fluidized bed.

b Fluidized-packed bed.

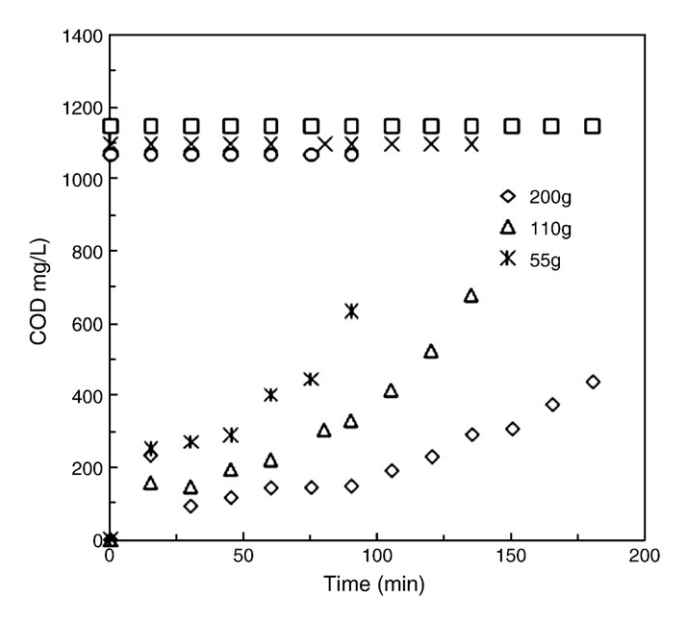
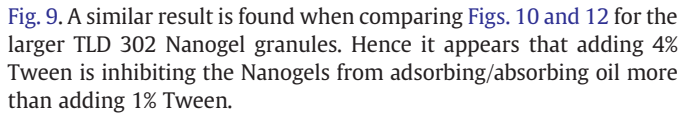


**Fig. 9.** Breakthrough curve in fluidized bed for 55 g, 110 g and 200 g TLD 301, 0.7–1.2 mm Nanogel granules when the proportion of Tween 80 is 1%, the inlet COD is around 1100 mg/L and  $U/U_{\rm mf}$  is 1.1.



The oil removal results from Table 6 also show that: (1) for the same type of Nanogel, when the flow rates are the same, the oil removal capacities become lower as the weight of the Nanogel granules increases. This is probably due to a decrease in the axial mixing of the solid phase as the bed height increases. (2) for the same  $U/U_{\rm mf}$  ratio and the same weight of Nanogel granules, it appears that the larger the particle size, the higher the oil removal capacity, and (3) the oil removal capacities for the same type of Nanogel are higher in

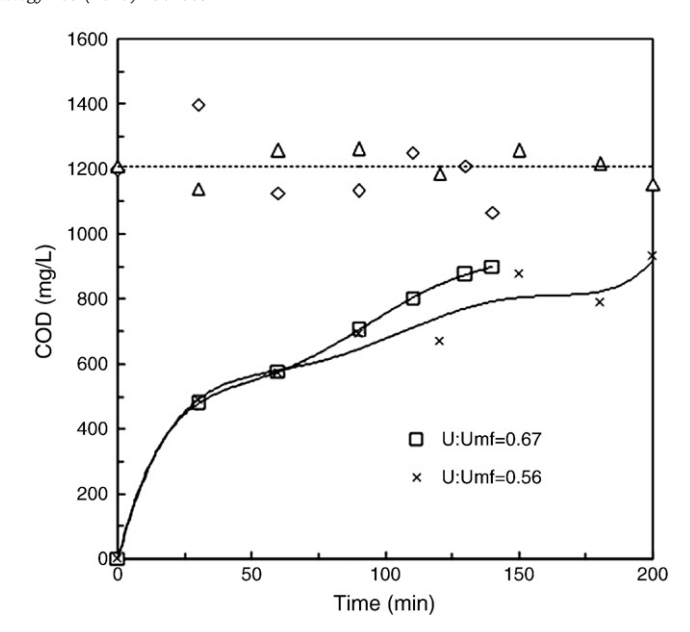


**Fig. 11.** Breakthrough curve in packed–fluidized bed for 55 g TLD 302, 1.7–2.35 mm Nanogel granules when the proportion of Tween 80 is 4%, the average inlet COD for both runs is around 1200 mg/L and  $U/U_{\rm mf}$  are 0.56 and 0.67, respectively.

the packed–fluidized bed mode than those in the fluidized bed. This latter result can be explained from the force balance Eq. (9). As Nanogels begin to absorb oil, the net buoyancy force acting on the particles decreases, (the buoyancy force is constant and the gravity force increases) and therefore the drag force ( $\Delta PA$ ) needed to fluidize the particles decreases and the bed begins to expand due to the increase of the gravity force. At the moment, when the length of the bed reaches the entire column or the sum of the gravity force and drag force is larger than the buoyancy force, the Nanogel particles begin to leave the column. For Nanogel particles which adsorb/absorb the same amount of oil in a fluidized bed or in a packed–fluidized bed, both will have the same gravity force and buoyancy force, but the

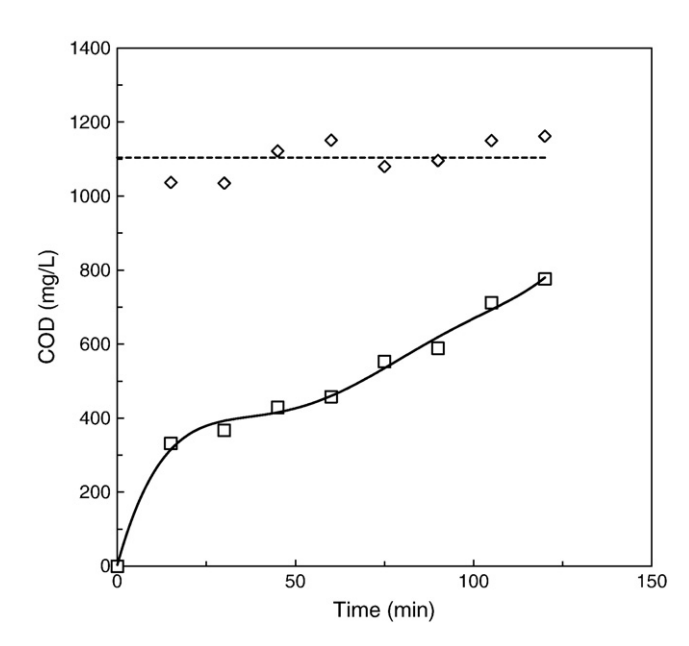


**Fig. 10.** Breakthrough curve in fluidized bed for 110 g TLD 302, 1.7–2.35 mm nanogel granules when the proportion of Tween 80 is 4%, the average inlet COD is around 1100 mg/L and  $U/U_{\rm mf}$  is 1.1.

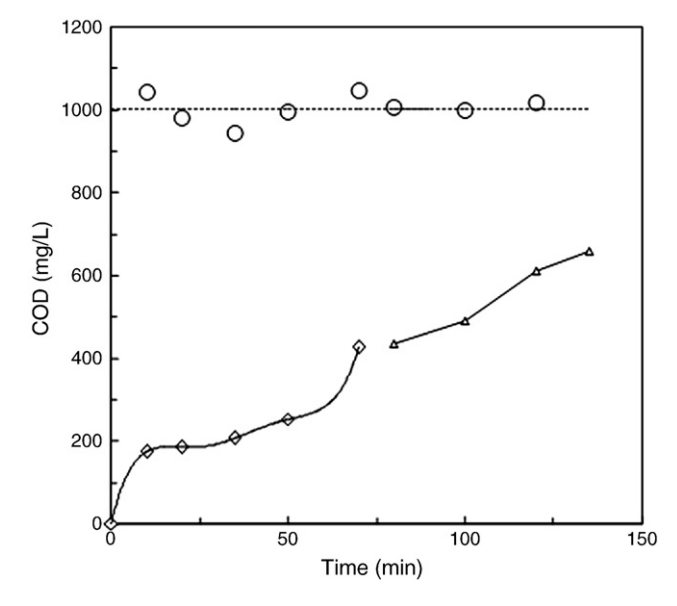


**Fig. 12.** Breakthrough curve in fluidized–packed bed for 110 g TLD 302, 1.7–2.35 mm Nanogel granules when the proportion of Tween 80 is 1%, the average inlet COD is around 1000 mg/L and  $U/U_{\rm mf}$  is 1.1 during the fluidized bed process and 0.67 during the packed bed process.

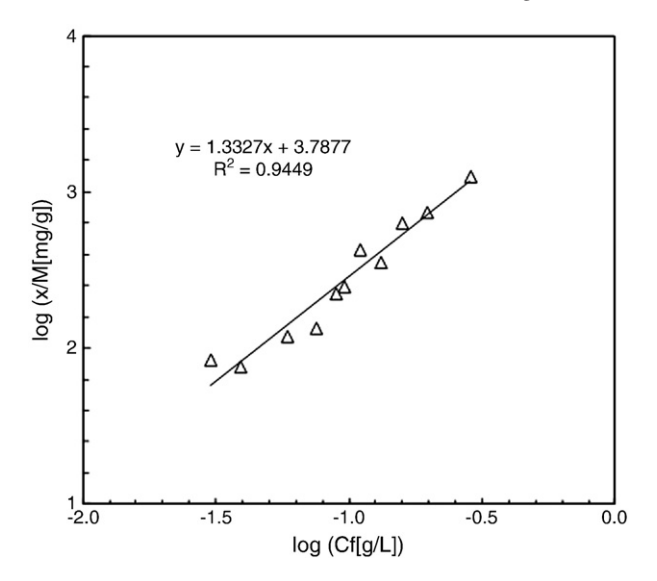


**Fig. 13.** Freundlich isotherm for adsorption of oil from oil-in-water emulsion by TLD 301 Nanogel granules.

former has the larger drag force due to the larger fluid velocity. Therefore it is much easier for the particles in the fluidized bed to leave the column when they adsorb/absorb the same amount of oil compared with the same particles in the packed-fluidized bed.

By decreasing the flow rate during an experiment (Fig. 12), the drag force is reduced (fluidized-packed bed mode) and the Nanogel granules will remain in the column for a longer time. This mode of operation will also result in a higher oil removal capacity.

## 4.6. Comparison of modeling results with experimental measurements

A Freundlich isotherm for oil adsorbed onto TLD 301 Nanogel from the oil-in-water emulsion using 4% Tween 80 as the stabilizer at room temperature is shown in Fig. 13. The Freundlich constants, k and 1/n, are calculated from the slope and intercept of the curve and are equal to 6133 and 1.33, respectively. One set of batch kinetic data fitted to the linear driving force model is shown in Fig. 14; the adsorption rate constant K' in Eq. (5) is obtained using a least squares regression. An average value of K', based on two separate batch kinetic experiments, is  $5.68 \times 10^{-2} \, \mathrm{s}^{-1}$ .

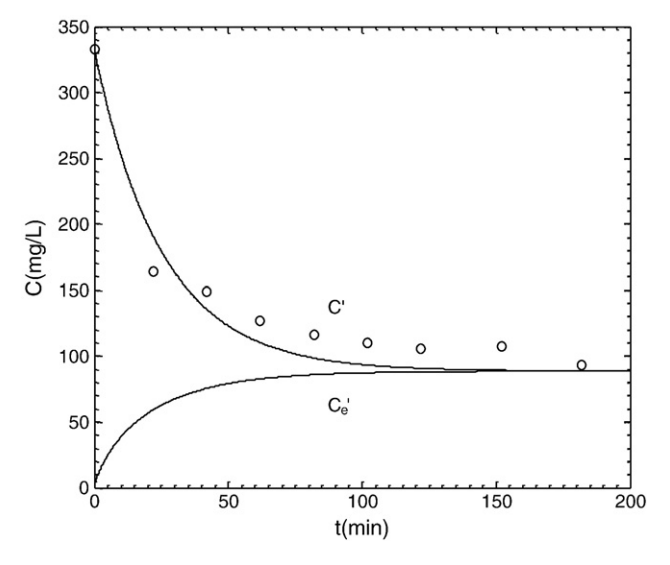


**Fig. 14.** Oil concentration as a function of time in a batch kinetic experiment: circles represent experimental data and solid lines C' and  $C'_e$  are obtained from the linear driving force model when K' is  $5.68 \times 10^{-2} \, \text{s}^{-1}$ .

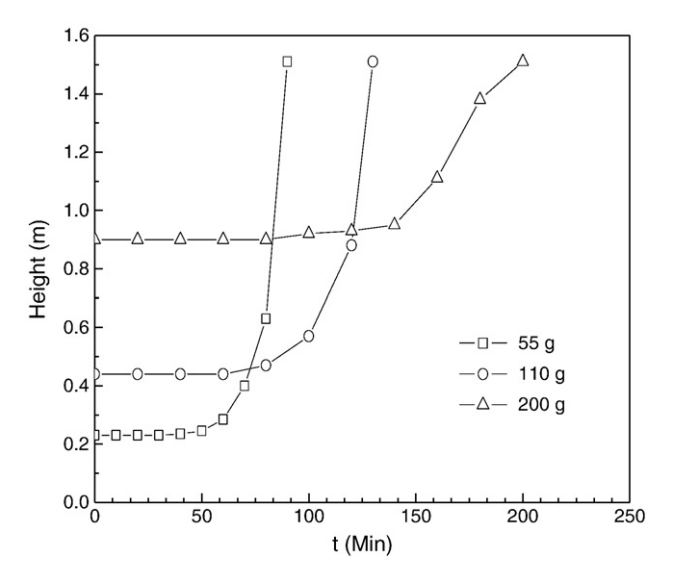


**Fig. 15.** Bed height as a function of time for 55 ( $\square$ ), 110 ( $\bigcirc$ ) and 200 ( $\triangle$ ) g of TLD 301. For 55 g TLD 301, data was fit by a horizontal line for t < 30 Min and a sixth order polynomial for t > 30 Min; for 110 g TLD 301, data was fit by a horizontal line for t < 60 Min and a fifth order polynomial for t > 60 Min; for 200 g TLD 301, data was fit by a horizontal line for t < 80 Min and a sixth order polynomial for t > 80 Min.

Unlike experiments in fluidized bed adsorbers reported in the literature, the expanded fluidized bed height in our experiments changes as a function of time. The fluidized bed height remains relatively constant at the beginning of the experiment until some of the Nanogels have adsorbed/absorbed an appreciable amount of oil. These particles become heavier and can no longer be suspended by the buoyancy force of the fluid, and the bed begins to expand downward towards the bottom of the column until the expanded bed height is equal to the physical length of the column at which point the experiment is stopped. Fig. 15 shows the expanded bed height data as a function of the time of the experiment for 55, 110, and 200 g of TLD 301 Nanogel. This adds an additional complication to the simulations.

The experimentally observed concentration of oil in the exit stream (breakthrough curve) is compared with the model predictions in Figs. 16 to 18. Here we have plotted the oil concentrations as actual mg/l rather than as COD mg/l using the calibration curve, Fig. 7, to convert from one to the other. All of the experimental runs in these three figures were made at the same conditions except for the weight

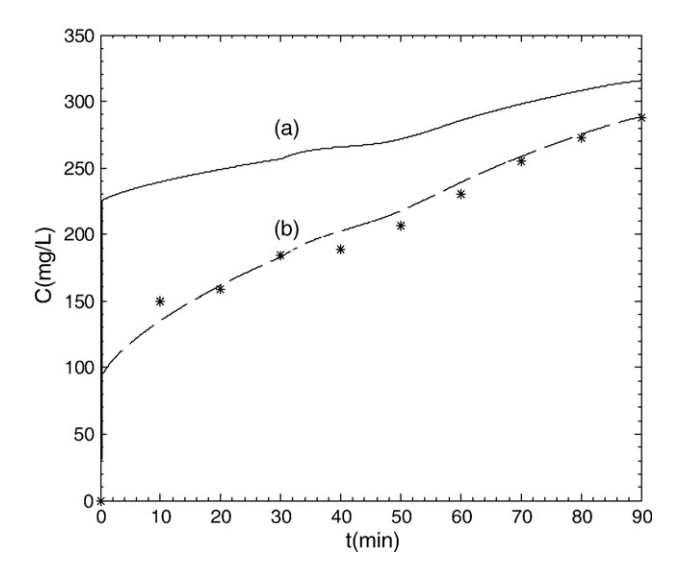


**Fig. 16.** Model results for the breakthrough curve using 55 g TLD 301: (a) measured K' (b) 2.75 K' compared to experimental data.

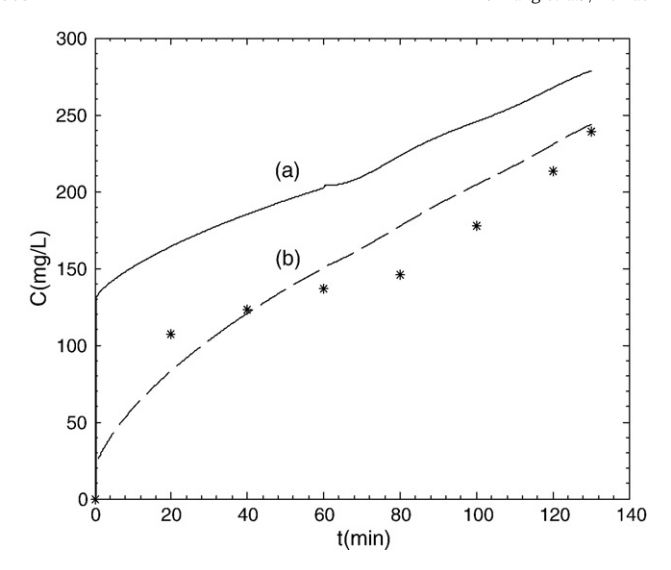


**Fig. 17.** Model results for the breakthrough curve using 110 g TLD 301: (a) measured *K'* (b) 2.75 *K'* compared to experimental data.

of Nanogel used (height of the bed). As seen in the figures, the results of the simulations and experiments are not in good agreement when using the value of  $K' = 5.68 \times 10^{-2} \, \mathrm{s}^{-1}$  as obtained from the batch kinetic experiments. We suspect that the K' value from the batch kinetic experiments is appreciably lower than the real K' value for adsorption in the fluidized bed, because the Nanogel particles are much better mixed in the fluidized bed than in the batch experiments performed in a bottle stirred by a shaker.

In the experimental run shown in Fig. 16 (55 g Nanogel, and the shortest bed height used), the value of K' which gives the best fit of the experimental breakthrough curve in the inverse fluidized bed was calculated by the method of least squares and is about 2.75 times larger  $(1.56 \times 10^{-1} \, \text{s}^{-1})$  than the original K' value. This new K' value is also used to fit the experimental data in Figs. 17 and 18, with poorer results observed as the bed height (amount of Nanogel granules) becomes larger. When less granules are used in the inverse fluidized bed (shorter bed), the Nanogel granules tend to saturate more uniformly because of the CSTR-like mixing. When more granules are fluidized in the bed, since the bed height is larger, it is more difficult

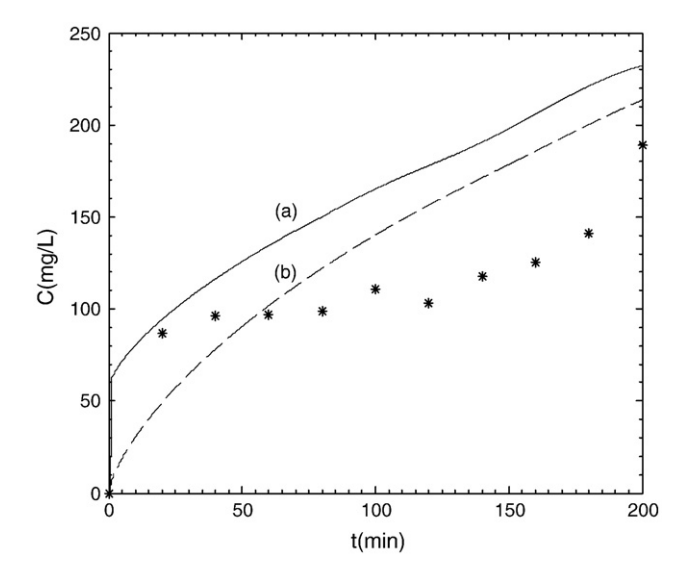


**Fig. 18.** Model results for the breakthrough curve using 200 g TLD 301: (a) measured K' (b) 2.75 K' compared to experimental data.

for the granules to mix well. In this case, the assumption made in the model that the solid phase is completely mixed is not very accurate.

# 5. Concluding remarks

The granule density and hydrodynamic characteristics of the Nanogels were calculated by measuring the pressure drop and bed expansion of clean water in the inverse fluidized bed. The experimental results are in good agreement with previous models used for liquid-solid fluidized beds. The main factors which affect the oil removal capacity of the Nanogel granules in the inverse fluidized bed and inverse packed-fluidized bed are the size of the granules, the bed height, and the fluid velocity. The use of Tween 80 to stabilize the oilin-water emulsions used in the experiments appears to decrease the adsorbing/absorbing capability of the Nanogels and the use of another type of stabilizer, perhaps a nanopowder (Pickering emulsion), should be investigated. A model was developed to predict the inverse fluidized bed experimental results based on equilibrium and kinetic batch measurements using the Nanogel and oil-in-water emulsion. The model assumed complete axial mixing in the solid phase, but variable bed height as a function of time. Good agreement between the model and experimental results are obtained for short bed heights using an equilibrium rate constant about 2.75 times larger than that measured in the batch system.

#### Acknowledgements

The authors gratefully acknowledge support for this research from the National Science Foundation through grant CBET 0730465. We also thank Cabot Corporation for supplying the Nanogel used in our experiments and purchasing a dedicated GC for our use. We thank Drs. Nirmalya Maity, Dhaval Doshi and A.J. Duplessis of Cabot Corporation for providing us with an industrial perspective as well as technical expertise and guidance.

#### References

- [1] J.W. Paterson, Wastewater Treatment Technology, Ann Arbor Science, Ann Arbor, Stoneham, MA, 1975.
- [2] R.F. Johnson, T.G. Manjrekar, H.R. Halligan, Removal of oil from water surface by sorption on unstructured fibers, Environ. Sci. Technol. 7 (1973) 439–443.
- [3] J.W. Paterson, Industrial wastewater treatment technology, Butterworth Publishers, second. ed.Stoneham, MA, 1985.
- [4] M. Quemeneur, Y. Marty, Fatty acids and sterols in domestic wastewaters, Water Res. 28 (1994) 1217–1226.
- [5] Manual on disposal of refining wastes, America Petroleum Institute, Washington. D. C., 1969, vol. 5, pp. 5–15.
- [6] G.F. Bennett, The removal of oil from wastewater by air flotation: a review, CRC Rev. Environ. Control 18 (1988) 189–253.
- [7] M.J. Ayotamuno, R.B. Kogbara, S.O.T. Ogaji, S.D. Probert, Petroleum contaminated ground-water: remediation using activated carbon, Appl. Energy 83 (2006) 1258–1264.
- [8] W. Jian, A. Kitanaka, W. Nishijima, A.U. Baes, M. Okada, Removal of oil pollutants in seawater as pretreatment of reverse osmosis desalination process, Wat. Res. 33 (1996) 1857–1863.
- [9] N. Moulai-Mostefa, A. Brou, L. Ding, M.Y. Joffrin, Ultrafiltration of oil in-water emulsions and cyclohexane microemulsions using a rotating disk system, Mecanique & Industries 6 (2005) 203–210.
- [10] J.D. Walker, R.R. Colwell, L. Petrakis, Degradation of petroleum by an alga, Prototheca zopfii, Appl. Microb. 30 (1975) 79–81.
- [11] A. Pasila, A biological oil adsorption filter, Mar. Pollut. Bull. 49 (2004) 1006–1012.
- [12] A. Cambiella, E. Ortea, G. Rios, J.M. Benito, C. Pazos, J. Coca, Treatment of oil-in-water emulsions: performance of a sawdust bed filter, J. Hazard. Mater. B131 (2006) 195–199.
- [13] G.R. Alther, Organically modified clay removes oil from water, Waste Manage. 15 (1995) 623–628.
- [14] T. Viraraghavam, H. Moazed, Removal of oil from water by bentonite, Fresenius Environment. Bull. 12 (2003) 1092–1097.
- [15] D. Mysore, T. Viraraghavan, Y. Jin, Treatment of oily waters using vermiculite, Water Res. 39 (2005) 2643–2653.
- [16] T.H. Ribeiro, J. Rubio, R.W. Smith, A dried hydrophobic aquaphyte as an oil filter for oil/water emulsions, Spill Sci. Technol. Bull. 8 (2003) 483–489.
- [17] D.O. Cooney, Adsorption Design for Wastewater Treatment, first ed.Boca Raton, Florida, 1999.

- [18] L.W. Hrubesh, P.R. Coronado, J.H. Satcher Jr., Solvent removal from water with hydrophobic aerogels, J. Non-Cryst, Solids 285 (2001) 328–332.
- [19] S. Standeker, Z. Novak, Z. Knez, Adsorption of toxic organic compounds from water with hydrophobic silica aerogels, J. Colloid Interface Sci. 310 (2007) 362–368.
- [20] J.G. Reynolds, P.R. Coronado, L.W. Hrubesh, Hydrophobic aerogels for oil-spill cleanup – intrinsic absorbing properties, Energy Source 23 (2001) 831–843.
- [21] J.G. Reynolds, P.R. Coronado, Hydrophobic aerogels for oil-spill cleanup synthesis and characterization, J. Non-Cryst. Solids 292 (2001) 127–137.
- [22] H. Liu, W. Sha, A.T. Cooperb, M. Fan, Preparation and characterization of a novel silica aerogel as adsorbent for toxic organic compounds, Colloids Surf. A: Physicochem. Eng. Aspects 347 (2009) 38–44.
- [23] J.F. Richardson, W.N. Zaki, Sedimentation and fluidization: Part I, Trans. Instn. Chem. Eng. 32 (1954) 35–53.
- [24] L.S. Fan, K. Muroyama, S.H. Chern, Hydrodynamic characteristics of inverse fluidization in liquid-solid and gas-liquid-solid systems, Chem. Eng. J. 24 (1982) 143–150.
- [25] R.J.F. Bendict, G. Kumaresan, M. Velan, Bed expansion and pressure drop studies in a liquid-solid inverse-fluidized bed reactor, Bioprocess Eng. 19 (1998) 137–142.
- [26] Y.J. Cho, H.Y. Park, S.W. Kim, Y. Kang, S.D. Kim, Heat transfer and hydrodynamics in two and three phase inverse fluidized beds, Ind. Eng. Chem. Res. 41 (2002) 2058–2063
- [27] Y.A.A. Ibrahim, C.L. Briens, A. Margarities, M.A. Bergongnou, Hydrodynamics characteristics of a three-phase inverse fluidized-bed column, AICHE J. 42 (1996) 1889–1900.
- [28] D.G. Karamanev, L.N. Nikolov, Bed expansion of liquid-solid inverse fluidization, AICHE J. 38 (1992) 1916–1922.

- [29] T. Rengannathan, K. Krishnaiah, Prediction of minimum fluidization velocity in two and three phase inverse fluidized beds, Can. J. Chem. Eng. 81 (2003) 853–860.
- [30] T. Rengannathan, K. Krishnaiah, Voidage characteristics and prediction of bed expansion in liquid–solid inverse fluidized bed. Chem. Eng. Sci. 60 (2005) 2545–2555.
- [31] T. Rengannathan, K. Krishnaiah, Stochastic simulation of hydrodynamics of a liquid-solid inverse fluidized bed, Ind. Eng. Chem. Res. 43 (2004) 4405–4412.
- [32] A.C.V. Lakshmi, M. Balamurugan, M. Sivakumar, T.N. Samuelm, M. Velan, Minimum fluidization velocity and friction factor in a liquid-solid inverse fluidized bed reactor. Bioprocess Eng. 22 (2000) 461–466.
- [33] I. Nikov, D. Karamanev, Liquid-solid mass transfer in inverse fluidized bed, AICHE I. 37 (1991) 781–784.
- [34] J.A. Quevedo, G. Patel, R. Pfeffer, Removal of oil from water by inverse fluidization of aerogels, Ind. Eng. Chem. Res. 48 (2009) 191–201.
- [35] A.M. Jirka, M.J. Carter, Reactor digestion method for COD analysis, Anal. Chem. 47 (1975) 1397
- [36] Method 8000: Reactor digestion method USEPA approved for oxygen chemical demand wastewater analysis, DR/890 Datalogging Colorimeter Handbook, Hach Co., Lovelanf, CO, 2004, pp. 427–436.
- [37] S. Veeraraghavan, L.T. Fan, A.P. Mathews, Modeling adsorption in liquid-solid fluidized beds, Chem. Eng. Sci. 44 (1989) 2333–2345.
- [38] P.R. Wright, B.J. Glasser, Modeling mass transfer and hydrodynamics in fluidizedbed adsorption of proteins, AICHE J. 47 (2001) 474–488.
- [39] R.A. Correa, L.A. Calcada, R.P. Pecanha, Development of a fluidized bed system for adsorption of phenol from aqueous solutions with commercial macroporous resins, Braz. J. Chem. Eng. 24 (2007) 15–28.
- [40] S.F. Chung, C.Y. Wen, Longitudinal dispersion of liquid flowing through fixed and fluidized beds, AICHE J. 14 (1968) 857–866.